Structure
Article

Single-Molecule Folding Mechanism of an EF-Hand Neuronal Calcium Sensor

Pétur O. Heidarsson,[1] Mariela R. Otazo,[2,3] Luca Bellucci,[2] Alessandro Mossa,[4] Alberto Imparato,[4] Emanuele Paci,[5] Stefano Corni,[2] Rosa Di Felice,[2] Birthe B. Kragelund,[1,*] and Ciro Cecconi[2,*]

[1]Structural Biology and NMR Laboratory, Department of Biology, University of Copenhagen, Ole Maaløes Vej 5, 2200 Copenhagen N, Denmark

[2]CNR Institute of Nanoscience S3, Via Giuseppe Campi, Modena 41125, Italy

[3]Department of Physics, Center of Applied Technologies and Nuclear Development (CEADEN), Calle 30, Number 502, Miramar, La Habana 11300, Cuba

[4]Department of Physics and Astronomy, University of Aarhus, Ny Munkegade, Building 1520, 8000 Aarhus C, Denmark

[5]Astbury Centre for Structural Molecular Biology, University of Leeds, Leeds LS2 9JT, UK

*Correspondence: bbk@bio.ku.dk (B.B.K.), ciro.cecconi@gmail.com (C.C.)

http://dx.doi.org/10.1016/j.str.2013.07.022

SUMMARY

EF-hand calcium sensors respond structurally to changes in intracellular Ca^{2+} concentration, triggering diverse cellular responses and resulting in broad interactomes. Despite impressive advances in decoding their structure-function relationships, the folding mechanism of neuronal calcium sensors is still elusive. We used single-molecule optical tweezers to study the folding mechanism of the human neuronal calcium sensor 1 (NCS1). Two intermediate structures induced by Ca^{2+} binding to the EF-hands were observed during refolding. The complete folding of the C domain is obligatory for the folding of the N domain, showing striking interdomain dependence. Molecular dynamics results reveal the atomistic details of the unfolding process and rationalize the different domain stabilities during mechanical unfolding. Through constant-force experiments and hidden Markov model analysis, the free energy landscape of the protein was reconstructed. Our results emphasize that NCS1 has evolved a remarkable complex interdomain cooperativity and a fundamentally different folding mechanism compared to structurally related proteins.

INTRODUCTION

EF-hand calcium binding proteins regulate diverse processes in almost every aspect of a cell life cycle. These proteins relay cellular changes of Ca^{2+} through intra- or interdomain rearrangements that allow them to interact with binding partners. Despite detailed structure characterization and elucidation of switch mechanisms in the native state (Capozzi et al., 2006; Grabarek, 2006), the folding mechanism of this large family of proteins is widely unexplored, with only a subset of systems studied (Aravind et al., 2008; Mukherjee et al., 2007; Stigler et al., 2011; Suarez et al., 2008; Yamniuk et al., 2007). To rationalize the conformational response of sensory EF-hand proteins to changes in Ca^{2+} concentration and its relation to function, the details of their folding mechanism can prove essential.

The emerging family of EF-hand neuronal calcium sensor (NCS) proteins currently includes 15 members. These are primarily expressed in neurons, except recoverin and guanylyl-cyclase-activating proteins, which are expressed in the retina (Ames and Lim, 2012; Burgoyne, 2004; Reyes-Bermudez et al., 2012). Neuronal calcium sensor 1 (NCS1) is the primordial member of the NCS family and is present in many organisms ranging from yeast to humans (Burgoyne, 2004). NCS1 is targeted to the plasma membrane by an N-terminal myristoylation group (McFerran et al., 1999) and is reported to bind an array of interaction partners (Burgoyne, 2007). It is involved in the regulation of neurotransmitter release (McFerran et al., 1999) and is linked to disorders such as schizophrenia (Koh et al., 2003) and autism (Piton et al., 2008), as well as to cognitive abilities such as learning and memory (Gomez et al., 2001; Handley et al., 2010; Saab et al., 2009; Weiss et al., 2010). Recently, functions in the young heart have also been reported (Nakamura et al., 2011). Two domains can be identified in NCS1 on the basis of its EF-hand motifs: the N domain (residues 1–94, α helices H1–H5) consisting of EF1 and EF2, and the C domain (residues 96–190, α helices H6–H9), consisting of EF3 and EF4 (Figure 1A). The two domains are separated by a short loop containing a conserved glycine that may act as a hinge, allowing domain movements (Heidarsson et al., 2012a). NCS1 is activated by binding three Ca^{2+} ions, which induces significant structuring from a predominantly molten-globule-like apo form, revealing a hydrophobic ligand-binding pocket spanning both domains (Aravind et al., 2008, Heidarsson et al., 2012a). While EF1 is unable to bind Ca^{2+} because of a conserved Cys-Pro mutation, EF2 and EF3 bind Ca^{2+} with high affinity and can also bind Mg^{2+} at resting conditions, whereas EF4 binds only Ca^{2+} and with lower affinity (Aravind et al., 2008). The folding mechanism of NCS1 has been characterized at equilibrium in bulk studies, showing individual cooperative domain unfolding with a less stable N domain (Aravind et al., 2008; Heidarsson et al., 2012a; Muralidhar et al., 2005). The kinetics and mechanistic details of the folding process have, however, remained elusive for the entire NCS family.

Deciphering the intricacies of protein folding pathways hidden in the ensemble average provided by traditional bulk techniques

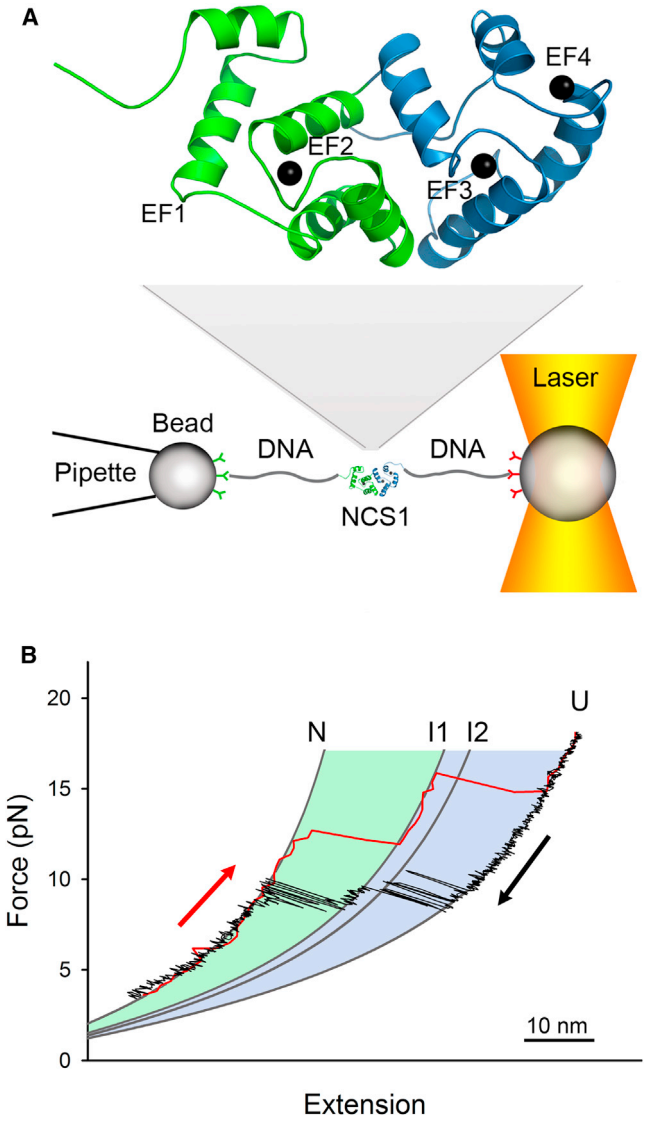

Figure 1. Manipulating Single NCS1 Molecules

(A) Solution structure of NCS1 (PDB code 2LCP) showing the two EF domains containing pairs of EF-hands (EF1-EF2 in green, EF3-EF4 in blue); EF-hands labeled EF2-EF4 have a Ca^{2+} ion bound (black spheres). NCS1 is manipulated with polystyrene beads by means of DNA molecular handles. During the experiment, the molecule is stretched and relaxed by moving the pipette.

(B) Force-versus-extension cycle showing stretching (red, 100 nm s^{-1}) and relaxing (black, 50 nm s^{-1}) of a NCS1 molecule. Folding from the unfolded state (U) to the native state (N) occurs via two detectable intermediate states, I1 and I2. Gray lines are WLC model fits to the data, and the green and blue shaded areas correspond to the N and C domains, respectively. Color-coded arrows indicate the pulling/relaxing directions. The unfolding from N to U occurs in a three-state manner, as state I1 is mechanically more stable than state I2 and unfolds at forces at which I2 cannot withstand the load.

See also Figures S1–S3.

is a daunting task. This is especially true when studying the complicated sequence of events that characterizes the folding mechanism of large multidomain proteins, such as NCS1. Different domains may fold at different rates via different pathways and may crosstalk through elaborate mechanisms that increase the level of complexity in the observed experimental signals. The advent of single-molecule techniques, such as optical tweezers, has provided an innovative perspective on the protein folding problem, allowing researchers to go beyond the ensemble average and dissect folding mechanisms in unprecedented detail (Borgia et al., 2008; Bustamante et al., 2004; Ritort, 2006; Schuler and Eaton, 2008). Using optical tweezers, it is now possible to follow the folding trajectories of individual proteins through mechanical manipulation and characterize the intermediate states populated by the molecule during its journey to the native state. (Bechtluft et al., 2007; Cecconi et al., 2005; Gao et al., 2012; Heidarsson et al., 2012b; Shank et al., 2010; Stigler et al., 2011). Conditions at which single-molecule manipulation experiments are performed, including the application of a force acting on the distance between two atoms, can be closely reproduced in silico. Molecular dynamics (MD) simulations and single-molecule force techniques have proved powerful and are complementary tools in characterizing unfolding at single-molecule level and in investigating the effect of mechanical forces on proteins (Forman et al., 2009; Marszalek et al., 1999; Schlierf et al., 2010).

Here, we use optical tweezers experiments and steered MD (SMD) simulation to study the folding and unfolding trajectories of individual NCS1 molecules and decipher the role in folding of each EF-hand Ca^{2+}-binding site. Under our experimental conditions, NCS1 exhibits a complex multistate folding mechanism characterized by a precise sequence of events induced by Ca^{2+} binding. Proper folding of EF3 and EF4 is a strict requirement for subsequent folding of the N domain. Under tension, the N domain is the first to unfold, followed at higher forces by the C domain. SMD simulation results reveal at the atomic level the sequence of events that lead to the mechanical unfolding of the molecule. Through constant-force experiments and hidden Markov model (HMM) data analysis, the salient features of the free energy landscape of NCS1 are reconstructed. The results demonstrate that NCS1 has a remarkably different folding mechanism from structurally related proteins.

RESULTS

NCS1 Folds through a Multistate Pathway

Single NCS1 molecules were manipulated by means of ~500 base pair double-stranded DNA handles that were attached to engineered cysteines, producing protein-DNA chimeric constructs (Figure 1A). A variant of NCS1 was generated in which Cys38 was replaced by serine and two cysteines were engineered at positions 4 and 188, effectively allowing force to be applied to the entire molecule in a controlled manner. This variant has very similar stability, fold, and calcium binding properties compared to the wild-type (WT) protein, as indicated by equilibrium unfolding experiments, nuclear magnetic resonance (NMR) spectroscopy, and Ca^{2+}-binding competition assays, respectively (Figure S1 available online).

Individual molecules were stretched and relaxed with a custom-built optical tweezers setup that operates by direct measurement of light momentum (Figure 1A; see Experimental Procedures for details). The kinetic profiles of NCS1 unfolding and refolding were characterized through constant-velocity experiments. Under our experimental conditions, we found that

NCS1 unfolds in an apparent three-state process and refolds in a four-state process via two distinct refolding intermediates, I1 and I2 (Figure 1B). Fluctuations between the different molecular states become more evident at slower stretching/relaxation speeds (Figure S2). Sometimes, I1 is too short lived to be detected in our traces (data not shown).

The differences in contour length (ΔL_c) associated with each refolding and unfolding transition were estimated by fitting 150 force-versus-extension curves with the worm-like-chain (WLC) model of polymer elasticity (Bustamante et al., 1994; Marko and Siggia, 1995). These model values, ΔL_c^{WLC} (gray lines in Figure 1B), were then compared to the nominal values, ΔL_c^0 (Cecconi et al., 2005; see Experimental Procedures for details). The decrease in contour length associated with the low force relaxing event (I1 to N) was estimated to be $\Delta L_c^{WLC} = 29 \pm 2$ nm (all errors are SDs), which is consistent with the refolding of the N domain ($\Delta L_c^0 = 30$ nm). On the other hand, ΔL_c^{WLC} estimated for the U to I2 and I2 to I1 transitions are 28 ± 2 nm and 6 ± 2 nm, respectively. Summed together (34 ± 3 nm), these values of ΔL_c^{WLC} are consistent with the refolding of the entire C domain ($\Delta L_c^0 =$ 33 nm). The WLC analysis of stretching traces yielded a ΔL_c^{WLC} of 30 ± 2 nm for the low force transition (N to I1) and ΔL_c^{WLC} of 34 ± 2 nm for the high force transition (I1 to U); these values are consistent, respectively with the unfolding of the N and C domains, respectively (see ΔL_c^0 above).

To further investigate which parts of the protein were involved in the different unfolding and refolding events, we generated two variants in which the sizes of the N and C domains were selectively altered. In $NCS1^{10Gly}$, ten glycine residues were inserted into an unstructured loop that connects EF3 and EF4, effectively changing the size of the C domain by 10%. In $NCS1^{38–188}$, no cysteine was engineered at position 4 and one DNA handle was attached directly to the native Cys38; in this way, only 56 residues of the N domain were subject to force, corresponding to ~40% change. Compared to NCS1, both for unfolding and refolding, the high force transitions were longer in $NCS1^{10Gly}$ and the low force transitions were shorter in $NCS1^{38–188}$ (Figure S3). These data, along with the WLC model fitting results, suggest that the C domain is mechanically more stable than the N domain and unfolds and refolds at higher forces. These observations are consistent with results obtained in bulk studies where the C domain was shown to be thermodynamically more stable than the N domain (Heidarsson et al., 2012a). Our single-molecule data also indicate that, while the N domain refolds in a single cooperative transition, the C domain folds in two steps. The size of these steps, however, is not consistent with the sequential folding of EF3 and EF4 hands. The change in contour length associated with the first refolding event should, in this case, be either 13.7 nm, if EF3 refolds first, or 16.2 nm, if EF4 refolds first; instead, it is 28 ± 2 nm. Hence, our data suggest a folding mechanism in which the C domain first undergoes a major conformational change (U to I2 transition), followed by a minor rearrangement (I2 to I1 transition) that leads to the native structure.

Role of EF-Hands in NCS1 Folding

We have shown that the folding pathway leading to the native state of NCS1 includes intermediate states, but the nature of the conformational changes that occur in these transitions has not been revealed. A reasonable possibility is that binding of Ca^{2+} ions into the EF sites induces or stabilizes these states. Binding of Ca^{2+} is known to cause conformational changes in EF-hands (Capozzi et al., 2006; Gifford et al., 2007), and in the absence of Ca^{2+}, the apo form of NCS1 has characteristics of a molten-globule-like conformation (Aravind et al., 2008). The canonical EF-hand has an ~12-residue binding loop where positions 1 and 12, which are invariably aspartates or glutamates, are necessary for calcium coordination (Gifford et al., 2007). For NCS1, these residues are D73/E84 (EF2), D109/E120 (EF3), and D157/E168 (EF4). To examine the role of Ca^{2+} binding in the folding of NCS1, we disabled each Ca^{2+} site individually (see Experimental Procedures and Supplemental Information) by mutating positions 1 and 12 to alanine and glutamine, respectively. This yielded the mutants $NCS1^{EF2}$, $NCS1^{EF3}$, and $NCS1^{EF4}$, where the superscript indicates the disabled EF site. The disruption of the calcium binding properties is apparent from the $^1H,^{15}N$-heteronuclear single quantum correlation (HSQC) peak positions and intensities of the glycine residues in position 6 in the binding loop, which have a characteristic downfield shifted chemical shift (Figures S1 and S4; Table S1). We then performed constant-velocity experiments on each of these variants.

As expected from the results described earlier, $NCS1^{EF2}$ clearly exhibited defective folding in the N domain (I1 to N transition) compared to NCS1, while C-domain folding (U to I1 transitions) apparently was unaltered, as it displayed similar contour length changes ($\Delta L_c^{WLC} = 32 \pm 2$ nm; number of events, n = 40), and it could still unfold at high force (Figures 2A and 3). The N domain could partially fold into a nonnative structure and would unfold at low force either gradually or in a sharp cooperative event. $NCS1^{EF3}$ force-versus-extension trajectories, on the other hand, displayed no detectable native transitions (Figure 2B). Both during relaxation and stretching, this variant displayed only small fluctuations that did not lead to globular or collapsed states. This behavior is consistent with results obtained in bulk (Muralidhar et al., 2005), where the stability of this variant resembled the apo state and where Ca^{2+} no longer exerted any stabilizing effect. Indeed, in our experiments, the apo form of NCS1 showed almost identical behavior to that of $NCS1^{EF3}$ (Figure 2B, inset). This is consistent with lowered $^1H,^{15}N$-HSQC peak intensities for the glycines in position 6 of the EF2 and EF4 binding loops for the $NCS1^{EF3}$ variant when compared to WT NCS1, $NCS1^{EF2}$, and $NCS1^{EF4}$, suggesting altered calcium affinity in the EF2 and EF4 binding sites (Figure S4; Table S1). The most interesting behavior was observed for $NCS1^{EF4}$. This variant always folded into I2 but could not fold into I1 (Figure 2C). In fact, the C domain of $NCS1^{EF4}$ showed only partial folding ($\Delta L_c^{WLC} = 29 \pm 3$ nm, N = 30) and did not display the same mechanical stability as in WT NCS1 (Figure 3). For this variant, at low forces (~6 pN), the N domain folded into a structure as compact as that of the native state ($\Delta L_c^{WLC} = 31 \pm 3$ nm, n = 25) (Figure 2C) but lacking its stability (Figure 3). These data indicate that Ca^{2+} binding to the EF4 site is responsible for the I2 → I1 transition and that it is mandatory for proper folding of both domains. Binding of Ca^{2+} to EF3 is instead responsible for the U → I2 transition and seems crucial for the conformational stability of the entire molecule. The behaviors displayed by the $NCS1^{EF2}$ and $NCS1^{EF4}$ variants confirm that the folding of the N domain is dependent on the folding of the C domain, whereas the C domain can fold

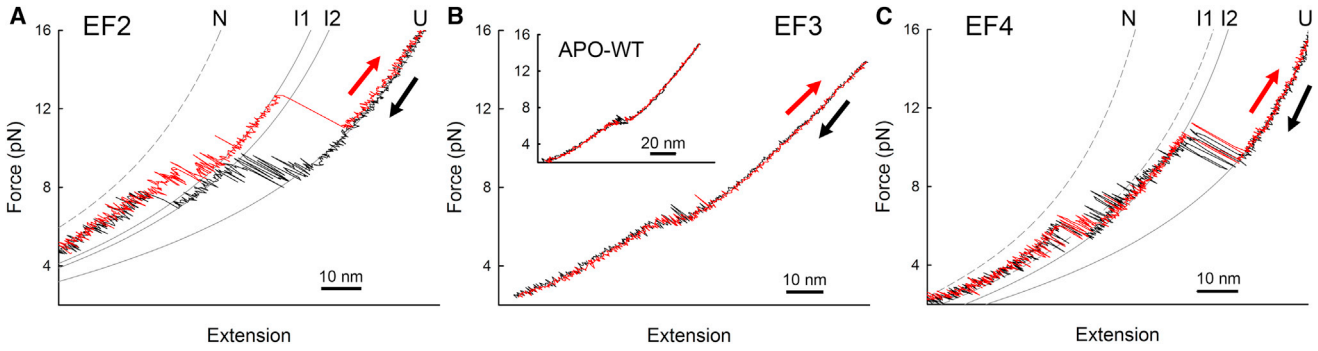

Figure 2. Unfolding/Refolding Trajectories of NCS1 Variants with Disabled Ca^{2+} Binding Sites

(A) Force-versus-extension cycle of $NCS1^{EF2}$ at 10 nm s^{-1}. The N domain is unable to fold correctly, while the C domain folds properly into both I2 and I1, as indicated by its mechanical strength and change in contour length on unfolding.

(B) Force-versus-extension cycle of $NCS1^{EF3}$ at 20 nm s^{-1}. Both the N and C domains failed to properly fold. The inset shows NCS1 folding in the absence of Ca^{2+}.

(C) Force-versus-extension cycle of $NCS1^{EF4}$ at 20 nm s^{-1}, showing the molecule folding into I2, but not into I1, and then at low force, the N domain folds into a structure that is similar in extension to its native state but mechanically weaker. Color-coded arrows indicate pulling/relaxing directions.

See also Figure S4 and Table S1.

independently. Notice that performing the experiments with the addition of 5 mM $MgCl_2$ did not change appreciably the unfolding/refolding behavior of the molecule (Figure S5).

Atomistic Simulations

A 0.7 μs all-atom SMD simulation has been performed to understand at the atomistic level the structure and the unfolding mechanism of the Ca^{2+}-bound state of NCS1 and to give deeper insight into the optical tweezers observations. The all-atom SMD simulation was performed in explicit solvent, starting from the NMR structure (Protein Data Bank [PDB] code 2LCP) retaining the calcium ions and solvated in 44952 TIP3P (Jorgensen et al., 1983) water molecules plus counterions to neutralize the system. The two termini of the protein were attached to ideal springs and pulled apart at a particularly low pulling speed of 0.5 Å/ns; see Experimental Procedures for details. Structural changes during the simulation were monitored by evaluating the distance root-mean-square (DRMS) deviation of the backbone with respect to the initial structure. DRMS deviations for the whole protein, N domain, and C domain are shown in Figure 4A (indicated in black, green, and blue, respectively). In agreement with experimental results, the SMD trajectory indicates that the N domain is mechanically less stable than the C domain (Figures 4A and 4B). During the first 150 ns, the C-terminal tail (residues 176–190) detached from the C domain. Subsequently, the N domain started losing its native structure: specifically, helix 1 (H1) detached from the protein core between 150 and 200 ns, followed by H2 in the subsequent 50 ns (Figure 4C). The unfolding of H2 competed with the detachment of H9 from the C domain. However, the C domain conserved its structure, as H9 remained stably "packed" between H6 and H8 and anchored to the protein core by the calcium binding site of EF4. Between 250 and 350 ns, the rest of the EF1-hand unfolded; namely, the loop between H2 and H3 (β1) was detached from the Ca^{2+}-binding site loop of EF2 (β3), and the H3 helix was detached from the rest of the protein (Figure 4C). During the detachment of β1, the H9 helix was partly disrupted. H9 was further disrupted as H4 unfolded between 400 ns and 500 ns. At 550 ns, the N domain (EF1 and EF2) was largely unfolded, EF3 was properly folded, and EF4 was partly disrupted (Figure 4C). New (nonnative) contacts are observed between residues 85–120 and 130–140 at 550 ns (see map in Figure 4B), which are due to the highly mobile loop connecting EF3 and EF4 approaching the protein core and the collapsing of the H6 and H8 occurring concurrently with the unfolding of the N domain (Figure 4C). Notice that the first unfolding event observed in the MD simulations—that is, the detachment of the C-terminal tail—concerns a region of the protein that is poorly defined in the NMR structure, as the last six residues had no observable nuclear Overhauser effects (NOEs) that could be used for distance restraints (Heidarsson et al., 2012a). Analysis of the MD unfolding trajectory reveals a key role played by the triple-helix structure H6-H9-H8 during the unfolding of NCS1. The H9 is docked between the H8 and H6 and anchored to the protein core by the calcium binding site of EF4. This triple-helix structure appears to be the main determinant of the mechanical stability of the C-domain, causing it to unfold at higher forces in the optical tweezers experiments.

Equilibrium Unfolding and Refolding Trajectories of NCS1

In constant-force experiments, NCS1 can be observed to fluctuate at equilibrium between different molecular states. In these experiments, the applied force is kept constant by a feedback mechanism while changes in the extension of the molecule, as it samples different conformations, are monitored in real time (Figure 5A). Using this technique, we collected 173 extension-versus-time traces from roughly 50 individual molecules. A distinct population shift from U to N is induced by decreasing the tension applied to the molecule. To extract thermodynamic and kinetic information, we analyzed each extension-versus-time trace individually by means of an adapted HMM algorithm (Rabiner, 1989), which estimates the transition rates between the different molecular states, together with the mean value and SD of the extension associated with them. In contrast to more traditional methods of analysis (i.e., discriminating the states on the basis of a set of selected thresholds), the HMM approach can distinguish between states very similar in

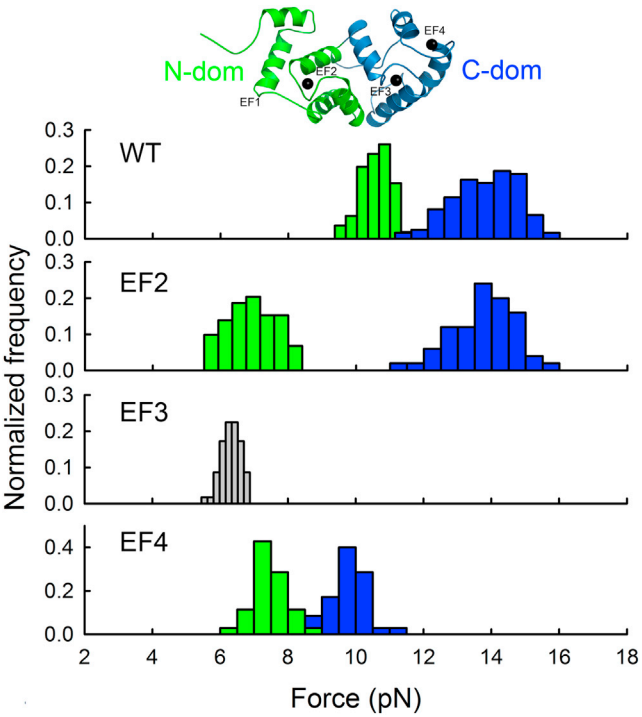

Figure 3. Unfolding Force Distributions for the N and C Domains of NCS1 and Its EF-Hand Variants

Force distributions are shown in green and blue for the N and C domains, respectively. The pulling speed was 100 nm s^{-1}. The N domain unfolds at 10.6 ± 0.6 pN for the WT (111 events, 12 molecules), 6.8 ± 0.8 pN for $NCS1^{EF2}$ (59 events, 4 molecules), and 7.4 ± 0.5 pN for $NCS1^{EF4}$ (35 events, 3 molecules). The C domain unfolds at 13.8 ± 1.0 pN for the WT (123 events, 11 molecules), 13.7 ± 0.9 pN for $NCS1^{EF2}$ (50 events, 4 molecules), and 9.8 ± 0.5 pN for $NCS1^{EF4}$ (35 events, 3 molecules). $NCS1^{EF3}$ displayed only a single low-force unfolding transition at the average force of 6.3 ± 0.3 pN (58 events, 3 molecules). Notice that addition of 5 mM $MgCl_2$ to the pulling buffer did not change appreciably the folding behavior of NCS1.

See also Figure S5.

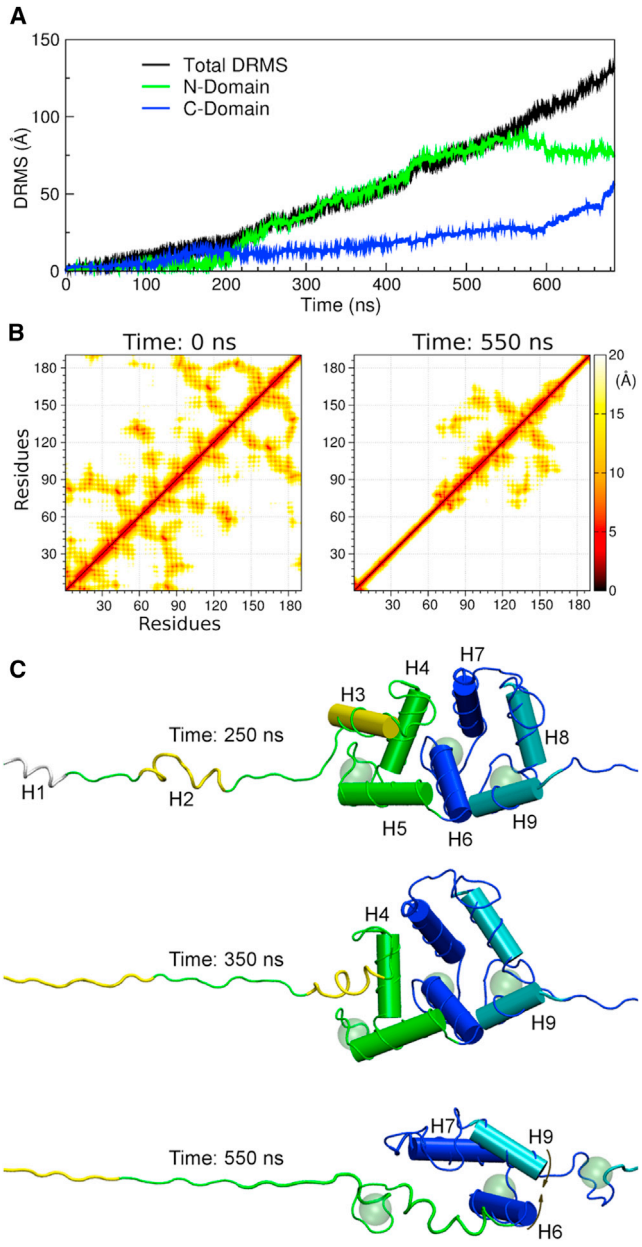

Figure 4. Steered MD Simulation of NCS1 Unfolding

(A) DRMS deviation for the whole NCS1 (black), the N domain (green), and the C domain (blue).

(B) Distance contact maps of the NCS1 Cα atoms evaluated at 0 and 550 ns. Distances are in angstroms.

(C) Snapshots of the simulated unfolding trajectory of NCS1 at 250 ns, 350 ns, and 550 ns. The alpha helices are labeled and shown in white (H1), yellow (H2 and H3), green (H4 and H5), blue (H6 and H7), and cyan (H8 and H9). Calcium ions are shown as light green spheres.

extension (such as I1 and I2) because it makes full use of the information about the time sequence of the observations.

From the rates, the salient features (energy of the intermediates, height and position of the barriers) of the free energy landscape can be reconstructed (Table 1; Figures 5B and S6). There are two direct tests of the accuracy of such reconstruction. First, the kinetic distances, as deduced by rates' analysis, compare very well to the observed jumps of the extension (Table S2). Second, the total unfolding free energy difference ΔG_{U-N} at zero external force, after subtracting the free energy of stretching, is 101 ± 9 kJ mol^{-1}, in agreement with the bulk spectroscopic measurement of 87 ± 16 kJ mol^{-1} (Figure S1). Collectively, the reconstructed landscape appears to be consistent with all our experimental results.

DISCUSSION

The most probable native folding pathway of NCS1, based on the aforementioned results, is depicted in Figure 6. During folding, and in a Ca^{2+}-dependent manner, the C domain (Figure 6, blue) collapses rapidly to a partially folded state (I2) consisting of a fully folded, Ca^{2+}-bound EF3 and a partially folded, Ca^{2+}-free EF4. Then, EF4 undergoes a conformational change upon binding a Ca^{2+}-ion, allowing proper folding of the C domain (I1). Only when this event has occurred can the N domain (Figure 6, green) rapidly collapse into its native state.

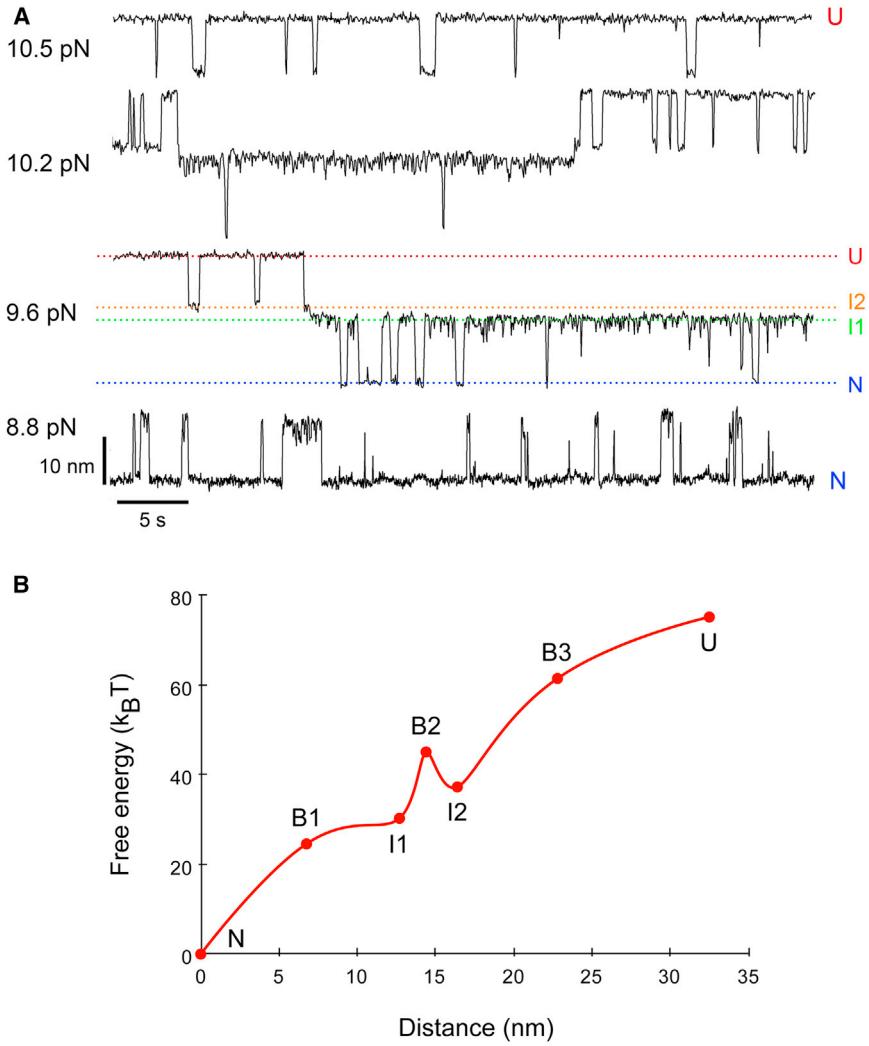

Figure 5. Constant-Force Experiments Reveal the Energy Landscape of NCS1

(A) Extension-versus-time traces of NCS1 at different preset force values. Force modulates the equilibrium between the different molecular species.

(B) Sketch of the free energy landscape at zero applied force, reconstructed using HMM analysis. The different NCS1 structural states are indicated together with the transition state barriers (B1-B2-B3) that separate them. The distances among the states are consistent both with the released molecular extension observed in hopping experiments and with the WLC model used to interpret pulling experiments.

See also Figure S6 and Table S2.

Our data suggest considerable interdomain crosstalk linked to Ca^{2+}-binding during NCS1 folding and significantly different folding kinetics of each EF domain. The rapid collapse of the N domain, subsequent to Ca^{2+} binding to EF4, is an example of cooperativity between EF domains. With respect to functioning as a calcium sensor, where structural changes in response to changes in cellular calcium concentration is a prerequisite (Nelson et al., 2001), the extreme conformational sensitivity of NCS1 relayed to the entire molecule as revealed by single-molecule experiments is an interesting property of this molecule. In the presence of Mg^{2+}, the calcium response of NCS1 will occur in the nM-μM range. The extreme cooperative folding of the two EF domains will enable NCS1 to become activated by a very small change in Ca^{2+} concentration in the cell, allowing it to function as a Ca^{2+} sensor with a threshold response.

The reconstructed energy landscape of Figure 5 shows that, at zero force, the U-to-I2 and I1-to-N transitions are downhill folding processes, as previously reported in similar experiments (Gebhardt et al., 2010), while the I2-to-I1 transition is a barrier-limited event (Gao et al., 2011). Notice that the height of the barriers in the reconstructed energy landscape depends on the assumptions that are made for the analysis of the constant force data, in particular on the value of the pre-exponential factor that is chosen (Gebhardt et al., 2010; Gao et al., 2011). The molecular rearrangements taking place during the folding process of NCS1 are not known. However, one can make speculations based on the observed changes in molecular extension and on the results of the simulation. Analysis of the SMD reveals how H9 affects the mechanical unfolding of the C domain. The H9, which forms part of the EF4 motif, is docked between H8 and H6 in an intricate aromatic ring arrangement (Figure 4). These interactions make H9 particularly stable, protecting the C domain from unfolding. One could speculate that H9 plays an important role also in the refolding process, driven by the hydrophobic collapse. The major conformational change observed during the U-to-I2 transition could lead to the formation of the docking site, while the I2-to-I1 transition could involve the docking of H9 between H6 and H8. In this sense, the last snapshot reported in Figure 4C, where the H6 and H8 are collapsed after the release of H9, could be a conformation close to the I2 state.

On comparison, it becomes apparent that the different members of the large family of EF-hand proteins have evolved different folding mechanisms, despite significant structural and sequential similarities. Three distinct domain-domain arrangements of proteins with four EF-hands (two pairs organized in two domains) have been observed, namely, the following: (1) Domains separated by a flexible linker that allows variable orientation of the domains with respect to each other (calmodulin [CaM] and related proteins), (2) domains separated by a short U-shaped linker placing EF-hands in a tandem array on one face of the protein (NCS family), and (3) domains organized in a compact globular fold with the two domains on opposite faces of the molecule (sarcoplasmic Ca^{2+}-binding proteins) (Gifford et al., 2007). The folding of CaM is the best characterized of all EF-hand proteins (Grabarek, 2011; Junker

Table 1. Reconstruction of the Free Energy Landscape of NCS1 at Zero External Force

Transition	$x^{\ddagger}_{\rightarrow}$ (nm)	$x^{\ddagger}_{\leftarrow}$ (nm)	$\Delta G/k_BT$	$\Delta G^{\ddagger}/k_BT$
N → I1	6.8 ± 0.2	5.9 ± 0.8	30 ± 2	25 ± 1
I1 → I2	1.7 ± 0.8	2 ± 1	7 ± 3	15 ± 2
I2 → U	6.4 ± 0.2	9.7 ± 0.2	37.8 ± 0.8	24 ± 1

Kinetic and thermodynamic quantities were measured from the force-dependence of transition rates. Errors are estimated from fit parameters' uncertainties. k_BT = 2.5 kJ mol^{-1}. Double daggers indicate the transition state.

and Rief, 2010; Lakowski et al., 2007; Rabl et al., 2002; Stigler and Rief, 2012; Stigler et al., 2011). A comparison of the structure and folding mechanisms of NCS1 and CaM under activating conditions is particularly interesting. On the single-molecule level, it has been demonstrated that the two domains of CaM can fold independently and in any order (Stigler et al., 2011). In contrast, NCS1 folds through a strict sequence of events, synchronized by ion binding, where the complete folding of the C domain is crucial for subsequent folding of the N domain. The difference in folding mechanism may stem from differences in the structural architecture of the two proteins. Both proteins have four EF-hands organized in two domains, but CaM has a somewhat symmetrical structure, with a long alpha helix separating the two almost identical N and C domains, which both bind two Ca^{2+} ions (Mikhaylova et al., 2011; Slavov et al., 2013). Instead, NCS1 is an asymmetrical molecule, as the N domain binds only one Ca^{2+} ion and there is significantly more interdomain contact (Figure 1A). These structural differences between CaM and NCS1 might be at the basis of their different folding mechanisms and may also be reflected in the functional profiles of the two proteins. CaM is known to bind more than 300 targets (Shen et al., 2005) and is ubiquitously expressed, while NCS1 is currently known to interact with approximately 20 proteins (Burgoyne and Haynes, 2012). The size difference between the two interactomes may be correlated with the restrictions imposed on the folding of NCS1 when compared to the relative freedom of CaM, which possibly allows CaM to sample a larger number of substates to accommodate different ligands.

NCS1 is an important protein for neurotransmitter release and for neuronal function, and its reaction to cellular cues is tightly linked to calcium concentrations. The intricacies of its folding pathway, revealed here from single-molecule optical tweezers experiments and SMD simulations, have revealed important interdomain cooperativity that shapes the ligand binding site, as well as a calcium sensitivity that should be examined further. A full repertoire of protein molecular behavior includes descriptions of folding and unfolding pathways and may help explain functional molecular responses.

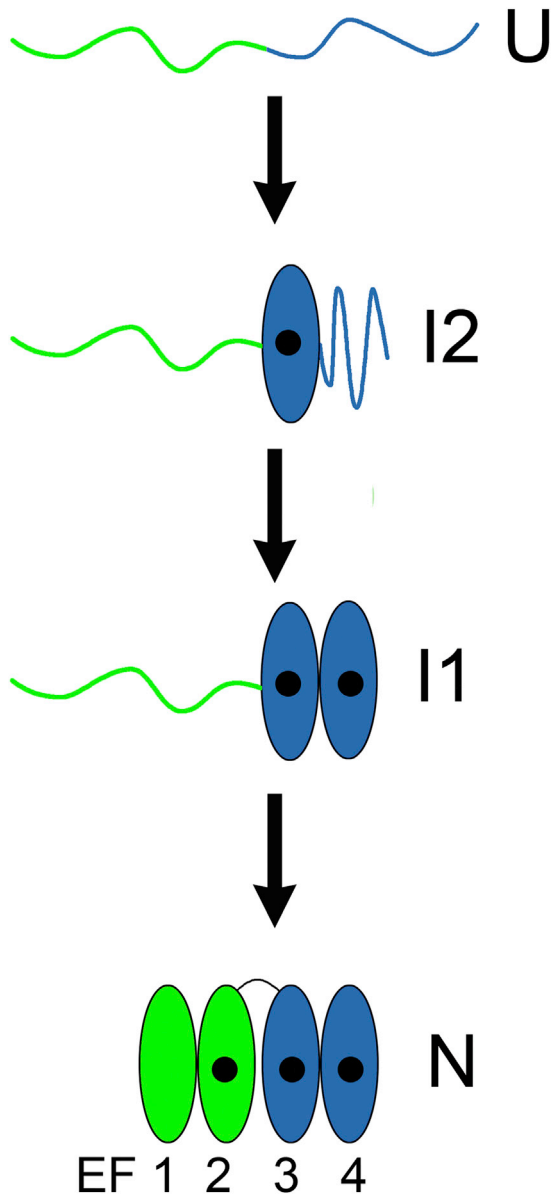

Figure 6. Folding Mechanism of NCS1
Schematic representation of the native folding pathway of NCS1 under tension is shown. The native state becomes increasingly populated at lower forces.

EXPERIMENTAL PROCEDURES

Protein-DNA Chimera Preparation

The double-cysteine constructs of NCS1 were engineered by using either a WT pET-16b or a pseudo-WT pET-16b expression plasmid (with Cys38 replaced by serine), by standard genetic techniques. The EF sites were individually disabled by introducing the D73A/E84Q (EF2), D109A/E120Q (EF3), or D157A/E168Q (EF4) mutations (De Cotiis et al., 2008; Woll et al., 2011; Aravind et al., 2008; Muralidhar et al., 2005; Jeromin et al., 2004). The *E. coli* strain BL21(DE3) was used to express unmyristoylated human NCS1 and variants and was grown at 37°C in Luria-Bertani medium. The protein was purified as described elsewhere (Kragelund et al., 2000), except for using protamine sulfate instead of streptomycin sulfate. Attachment of DNA to proteins and coupling of protein-DNA chimeras to beads was performed exactly as in previous work (Cecconi et al., 2008). As criteria for choosing attachment sites, we aimed to: (1) interfere as little as possible with the chemical composition of the protein by performing, whenever possible, serine-to-cysteine mutations; and (2) minimize the probability of a perturbation from the DNA handles by making mutations distant to the structured regions. In the N terminus, the closest serine is in position 4; thus, it was chosen as attachment site. On the other end, in the C terminus, the closest serine is Ser178, close to the structured part of the C domain. As a consequence, for the C domain, we chose Gly188 as attachment point, because changing Leu189 or Val190 would have changed the residue from highly hydrophobic to polar.

Optical Tweezers Experiments

All experiments were performed using a custom-built optical tweezers instrument with a dual-beam laser trap of 840 nm wavelength (Heidarsson et al., 2012b). The experiments were conducted at ambient temperatures in 10 mM Tris, 250 mM NaCl, 10 mM $CaCl_2$ at pH 7.0, or in the same buffer with 0.5 mM EGTA excluding $CaCl_2$, for measurements on the apo form of NCS1. During the experiment, a 3.10 μm antidigoxigenin-coated bead (Spherotec) was held in the optical trap, while a 2.18 μm streptavidin-coated bead (Spherotec) was held at the end of a micropipette by suction. The force applied on the molecule was varied by moving the micropipette toward or away from the optical trap by means of a piezoelectric flexure stage (MAX311/M, Thorlabs). The applied force was determined by measuring the change in light momentum of the laser beams leaving the trap (Smith et al., 2003). Changes in the extension of the molecule were determined by measuring the distance between the two beads (Smith et al., 2003). Constant-velocity traces were collected at constant speeds from 5 to 1,000 nm s^{-1}. Force and extension of the molecule were recorded at a rate of 40 Hz. Only those molecules that displayed the characteristic DNA overstretching transition at 67 pN were used in the analysis (Cecconi et al., 2005).

In constant-force experiments, the force applied on the molecule was kept constant through a force-feedback mechanism. The average force was measured and compared to the desired force every 1 ms. Any difference between these forces was compensated by moving the micropipette with the piezoelectric flexure stage. In constant-force experiments, the applied force and molecule extension were recorded at a rate of 100 Hz.

Changes in Contour Length

Nominal changes in contour lengths upon unfolding/refolding of NCS1 were calculated as described elsewhere (Cecconi et al., 2005). Distances between the Cα atoms in the corresponding residues in the native state were measured using the solution structure of NCS1 (PDB code 2LCP). In partially unfolded conformations, the length of the folded regions was determined using the coordinates of 2LCP. The nominal contour length of each molecular state was determined as L_c^0 = length of the folded region + (number of unfolded residues × 0.36 nm). On an unfolding or refolding event, ΔL_c was evaluated as the difference in length of the protein before and after the transition.

MD Simulations

MD simulations were performed with NAMD (v2.8) (Phillips et al., 2005), by using the CHARMM27 force field (MacKerell et al., 1998) for the protein and the counterions and the TIP3P (Jorgensen et al., 1983) force field for water. An unrestrained 8 ns simulation was performed starting from the first structure of the NMR solution structures (PDB code 2LCP) (Heidarsson et al., 2012a). The equilibrated structure was then used as the starting point for the SMD simulation. In a SMD simulation, the two termini are connected to an ideal spring with an elastic constant of 0.5 kcal/(mol $Å^2$), and pulled apart at a speed of 0.5 Å/ns. The full unfolding of the protein required a total simulation time of 0.7 μs (corresponding to about 500,000 hr of central processing units). A detailed description of the simulation setup can be found in the Supplemental Experimental Procedures.

HMM Analysis

HMM algorithms are a tool of choice for the interpretation of single-molecule observed time series, either from fluorescence spectroscopy (Andrec et al., 2003) or optical tweezers (Chodera et al., 2011). In our case, the use of HMM is crucial because the two intermediates I1 and I2 could hardly be discriminated based solely on the difference between their end-to-end extensions. A total of 173 extension-versus-time traces from roughly 50 molecules were used in our landscape reconstruction, with values of the constant force ranging from 8.3 pN to 10.7 pN. The shortest trace lasted 22 s, and the longest trace lasted 2,800 s. More details about the data analysis procedure are described in the Supplemental Experimental Procedures.

SUPPLEMENTAL INFORMATION

Supplemental information includes Supplemental Experimental Procedures, six figures, and two tables and can be found with this article online at http://dx.doi.org/10.1016/j.str.2013.07.022.

ACKNOWLEDGMENTS

P.O.H. and B.B.K. thank the Carlsberg Foundation for financial support. A.M. and A.I. gratefully acknowledge financial support from the Lundbeck Foundation. S.A. Sjørup is thanked for excellent technical assistance. C.C. gratefully acknowledges financial support from Fondazione Cassa di Risparmio di Modena, the European Union through a Marie Curie International Re-Integration grant (no. 44952), the Italian Ministry of Education, University, and Research (MIUR; grant no. 17DPXLNBEK), and partial support from the Italian MIUR FIRB RBPR05JH2P "ITALNANONET" project. M.R.O. gratefully acknowledges financial support from the Abdus Salam International Centre for Theoretical Physics, Training and Research in Italian Laboratories program. E.P. and L.B. acknowledge support from HPC-Europa2. R.D.F., S.C., and L.B. acknowledge financial support from the Italian Institute of Technology through Project MOPROSURF as well as the computational platform and computational support from CINECA (Bologna, Italy). We also thank Prof. E. Molinari and Dr. P. Facci for their insightful discussions.

Received: March 7, 2013
Revised: July 13, 2013
Accepted: July 28, 2013
Published: September 5, 2013

REFERENCES

Ames, J.B., and Lim, S. (2012). Molecular structure and target recognition of neuronal calcium sensor proteins. Biochim. Biophys. Acta *1820*, 1205–1213.

Andrec, M., Levy, R.M., and Talaga, D.S. (2003). Direct Determination of Kinetic Rates from Single-Molecule Photon Arrival Trajectories Using Hidden Markov Models. J. Phys. Chem. A *107*, 7454–7464.

Aravind, P., Chandra, K., Reddy, P.P., Jeromin, A., Chary, K.V., and Sharma, Y. (2008). Regulatory and structural EF-hand motifs of neuronal calcium sensor-1: Mg^{2+} modulates Ca^{2+} binding, Ca^{2+} -induced conformational changes, and equilibrium unfolding transitions. J. Mol. Biol. *376*, 1100–1115.

Bechtluft, P., van Leeuwen, R.G., Tyreman, M., Tomkiewicz, D., Nouwen, N., Tepper, H.L., Driessen, A.J., and Tans, S.J. (2007). Direct observation of chaperone-induced changes in a protein folding pathway. Science *318*, 1458–1461.

Borgia, A., Williams, P.M., and Clarke, J. (2008). Single-molecule studies of protein folding. Annu. Rev. Biochem. *77*, 101–125.

Burgoyne, R.D. (2004). The neuronal calcium-sensor proteins. BBA-Mol. Cell Res. *1742*, 59–68.

Burgoyne, R.D. (2007). Neuronal calcium sensor proteins: generating diversity in neuronal Ca^{2+} signalling. Nat. Rev. Neurosci. *8*, 182–193.

Burgoyne, R.D., and Haynes, L.P. (2012). Understanding the physiological roles of the neuronal calcium sensor proteins. Mol. Brain *5*, 2.

Bustamante, C., Marko, J.F., Siggia, E.D., and Smith, S. (1994). Entropic elasticity of lambda-phage DNA. Science *265*, 1599–1600.

Bustamante, C., Chemla, Y.R., Forde, N.R., and Izhaky, D. (2004). Mechanical processes in biochemistry. Annu. Rev. Biochem. *73*, 705–748.

Capozzi, F., Casadei, F., and Luchinat, C. (2006). EF-hand protein dynamics and evolution of calcium signal transduction: an NMR view. J. Biol. Inorg. Chem. *11*, 949–962.

Cecconi, C., Shank, E.A., Bustamante, C., and Marqusee, S. (2005). Direct observation of the three-state folding of a single protein molecule. Science *309*, 2057–2060.

Cecconi, C., Shank, E.A., Dahlquist, F.W., Marqusee, S., and Bustamante, C. (2008). Protein-DNA chimeras for single molecule mechanical folding studies with the optical tweezers. Eur. Biophys. J. *37*, 729–738.

Chodera, J.D., Elms, P.J., Noé, F., Keller, B., Kaiser, C.M., Ewall-Wice, A., Marqusee, S., Bustamante, C., and Hinrichs, N.S. (2011). Bayesian hidden Markov model analysis of single-molecule force spectroscopy: characterizing kinetics under measurement uncertainty. arXiv, arXiv:1108.1430, http://arxiv.org/abs/1108.1430.

De Cotiis, D.A., Woll, M.P., Fox, T.E., Hill, R.B., Levenson, R., and Flanagan, J.M. (2008). Optimized expression and purification of myristoylated human neuronal calcium sensor 1 in E. coli. Protein Expr. Purif. *61*, 103–112.

Forman, J.R., Yew, Z.T., Qamar, S., Sandford, R.N., Paci, E., and Clarke, J. (2009). Non-native interactions are critical for mechanical strength in PKD domains. Structure *17*, 1582–1590.

Gao, Y., Sirinakis, G., and Zhang, Y. (2011). Highly anisotropic stability and folding kinetics of a single coiled coil protein under mechanical tension. J. Am. Chem. Soc. *133*, 12749–12757.

Gao, Y., Zorman, S., Gundersen, G., Xi, Z., Ma, L., Sirinakis, G., Rothman, J.E., and Zhang, Y. (2012). Single reconstituted neuronal SNARE complexes zipper in three distinct stages. Science *337*, 1340–1343.

Gebhardt, J.C., Bornschlögl, T., and Rief, M. (2010). Full distance-resolved folding energy landscape of one single protein molecule. Proc. Natl. Acad. Sci. USA *107*, 2013–2018.

Gifford, J.L., Walsh, M.P., and Vogel, H.J. (2007). Structures and metal-ion-binding properties of the Ca^{2+}-binding helix-loop-helix EF-hand motifs. Biochem. J. *405*, 199–221.

Gomez, M., De Castro, E., Guarin, E., Sasakura, H., Kuhara, A., Mori, I., Bartfai, T., Bargmann, C.I., and Nef, P. (2001). Ca^{2+} signaling via the neuronal calcium sensor-1 regulates associative learning and memory in C. elegans. Neuron *30*, 241–248.

Grabarek, Z. (2006). Structural basis for diversity of the EF-hand calcium-binding proteins. J. Mol. Biol. *359*, 509–525.

Grabarek, Z. (2011). Insights into modulation of calcium signaling by magnesium in calmodulin, troponin C and related EF-hand proteins. Biochim. Biophys. Acta *1813*, 913–921.

Handley, M.T., Lian, L.Y., Haynes, L.P., and Burgoyne, R.D. (2010). Structural and functional deficits in a neuronal calcium sensor-1 mutant identified in a case of autistic spectrum disorder. PLoS ONE *5*, e10534.

Heidarsson, P.O., Bjerrum-Bohr, I.J., Jensen, G.A., Pongs, O., Finn, B.E., Poulsen, F.M., and Kragelund, B.B. (2012a). The C-terminal tail of human neuronal calcium sensor 1 regulates the conformational stability of the Ca^{2+}-activated state. J. Mol. Biol. *417*, 51–64.

Heidarsson, P.O., Valpapuram, I., Camilloni, C., Imparato, A., Tiana, G., Poulsen, F.M., Kragelund, B.B., and Cecconi, C. (2012b). A highly compliant protein native state with a spontaneous-like mechanical unfolding pathway. J. Am. Chem. Soc. *134*, 17068–17075.

Jeromin, A., Muralidhar, D., Parameswaran, M.N., Roder, J., Fairwell, T., Scarlata, S., Dowal, L., Mustafi, S.M., Chary, K.V.R., and Sharma, Y. (2004). N-terminal myristoylation regulates calcium-induced conformational changes in neuronal calcium sensor-1. J. Biol. Chem. *279*, 27158–27167.

Jorgensen, W.L., Chandrasekhar, J., Madura, J.D., Impey, R.W., and Klein, M.L. (1983). Comparison of simple potential functions for simulating liquid water. J. Chem. Phys. *79*, 926–935.

Junker, J.P., and Rief, M. (2010). Evidence for a broad transition-state ensemble in calmodulin folding from single-molecule force spectroscopy. Angew. Chem. Int. Ed. Engl. *49*, 3306–3309.

Koh, P.O., Undie, A.S., Kabbani, N., Levenson, R., Goldman-Rakic, P.S., and Lidow, M.S. (2003). Up-regulation of neuronal calcium sensor-1 (NCS-1) in the prefrontal cortex of schizophrenic and bipolar patients. Proc. Natl. Acad. Sci. USA *100*, 313–317.

Kragelund, B.B., Hauenschild, A., Carlström, G., Pongs, O., and Finn, B.E. (2000). 1H, 13C, and 15N assignments of un-myristoylated Ca^{2+}-frequenin, a synaptic efficacy modulator. J. Biomol. NMR *16*, 85–86.

Lakowski, T.M., Lee, G.M., Okon, M., Reid, R.E., and McIntosh, L.P. (2007). Calcium-induced folding of a fragment of calmodulin composed of EF-hands 2 and 3. Protein Sci. *16*, 1119–1132.

MacKerell, A.D., Bashford, D., Bellott, M., Dunbrack, R.L., Evanseck, J.D., Field, M.J., Fischer, S., Gao, J., Guo, H., Ha, S., et al. (1998). All-atom empirical potential for molecular modeling and dynamics studies of proteins. J. Phys. Chem. B *102*, 3586–3616.

Marko, J.F., and Siggia, E.D. (1995). Statistical mechanics of supercoiled DNA. Phys. Rev. E Stat. Phys. Plasmas Fluids Relat. Interdiscip. Topics *52*, 2912–2938.

Marszalek, P.E., Lu, H., Li, H., Carrion-Vazquez, M., Oberhauser, A.F., Schulten, K., and Fernandez, J.M. (1999). Mechanical unfolding intermediates in titin modules. Nature *402*, 100–103.

McFerran, B.W., Weiss, J.L., and Burgoyne, R.D. (1999). Neuronal $Ca^{(2+)}$ sensor 1. Characterization of the myristoylated protein, its cellular effects in permeabilized adrenal chromaffin cells, $Ca^{(2+)}$-independent membrane association, and interaction with binding proteins, suggesting a role in rapid $Ca^{(2+)}$ signal transduction. J. Biol. Chem. *274*, 30258–30265.

Mikhaylova, M., Hradsky, J., and Kreutz, M.R. (2011). Between promiscuity and specificity: novel roles of EF-hand calcium sensors in neuronal Ca^{2+} signalling. J. Neurochem. *118*, 695–713.

Mukherjee, S., Mohan, P.M., Kuchroo, K., and Chary, K.V. (2007). Energetics of the native energy landscape of a two-domain calcium sensor protein: distinct folding features of the two domains. Biochemistry *46*, 9911–9919.

Muralidhar, D., Jobby, M.K., Krishnan, K., Annapurna, V., Chary, K.V., Jeromin, A., and Sharma, Y. (2005). Equilibrium unfolding of neuronal calcium sensor-1: N-terminal myristoylation influences unfolding and reduces protein stiffening in the presence of calcium. J. Biol. Chem. *280*, 15569–15578.

Nakamura, T.Y., Jeromin, A., Mikoshiba, K., and Wakabayashi, S. (2011). Neuronal calcium sensor-1 promotes immature heart function and hypertrophy by enhancing Ca^{2+} signals. Circ. Res. *109*, 512–523.

Nelson, M.R., Chagot, B., and Chazin, W.J. (2001). EF-Hand Calcium-Binding Proteins (New York: John Wiley & Sons).

Phillips, J.C., Braun, R., Wang, W., Gumbart, J., Tajkhorshid, E., Villa, E., Chipot, C., Skeel, R.D., Kalé, L., and Schulten, K. (2005). Scalable molecular dynamics with NAMD. J. Comput. Chem. *26*, 1781–1802.

Piton, A., Michaud, J.L., Peng, H., Aradhya, S., Gauthier, J., Mottron, L., Champagne, N., Lafrenière, R.G., Hamdan, F.F., Joober, R., et al.; S2D team. (2008). Mutations in the calcium-related gene IL1RAPL1 are associated with autism. Hum. Mol. Genet. *17*, 3965–3974.

Rabiner, L.R. (1989). A tutorial on hidden Markov models and selected applications in speech recognition. Proc. IEEE *77*, 257–286.

Rabl, C.R., Martin, S.R., Neumann, E., and Bayley, P.M. (2002). Temperature jump kinetic study of the stability of apo-calmodulin. Biophys. Chem. *101-102*, 553–564.

Reyes-Bermudez, A., Miller, D.J., and Sprungala, S. (2012). The Neuronal Calcium Sensor protein Acrocalcin: a potential target of calmodulin regulation during development in the coral Acropora millepora. PLoS ONE *7*, e51689.

Ritort, F. (2006). Single-molecule experiments in biological physics: methods and applications. J. Phys. Condens. Matter *18*, R531–R583.

Saab, B.J., Georgiou, J., Nath, A., Lee, F.J., Wang, M., Michalon, A., Liu, F., Mansuy, I.M., and Roder, J.C. (2009). NCS-1 in the dentate gyrus promotes exploration, synaptic plasticity, and rapid acquisition of spatial memory. Neuron *63*, 643–656.

Schlierf, M., Yew, Z.T., Rief, M., and Paci, E. (2010). Complex unfolding kinetics of single-domain proteins in the presence of force. Biophys. J. *99*, 1620–1627.

Schuler, B., and Eaton, W.A. (2008). Protein folding studied by single-molecule FRET. Curr. Opin. Struct. Biol. *18*, 16–26.

Shank, E.A., Cecconi, C., Dill, J.W., Marqusee, S., and Bustamante, C. (2010). The folding cooperativity of a protein is controlled by its chain topology. Nature *465*, 637–640.

Shen, X., Valencia, C.A., Szostak, J.W., Dong, B., and Liu, R. (2005). Scanning the human proteome for calmodulin-binding proteins. Proc. Natl. Acad. Sci. USA *102*, 5969–5974.

Slavov, N., Carey, J., and Linse, S. (2013). Calmodulin transduces Ca(2+) oscillations into differential regulation of its target proteins. ACS Chem. Neurosci. *4*, 601–612.

Smith, S.B., Cui, Y., and Bustamante, C. (2003). Optical-trap force transducer that operates by direct measurement of light momentum. Methods Enzymol. *361*, 134–162.

Stigler, J., and Rief, M. (2012). Calcium-dependent folding of single calmodulin molecules. Proc. Natl. Acad. Sci. USA *109*, 17814–17819.

Stigler, J., Ziegler, F., Gieseke, A., Gebhardt, J.C., and Rief, M. (2011). The complex folding network of single calmodulin molecules. Science *334*, 512–516.

Suarez, M.C., Rocha, C.B., Sorenson, M.M., Silva, J.L., and Foguel, D. (2008). Free-energy linkage between folding and calcium binding in EF-hand proteins. Biophys. J. *95*, 4820–4828.

Weiss, J.L., Hui, H., and Burgoyne, R.D. (2010). Neuronal calcium sensor-1 regulation of calcium channels, secretion, and neuronal outgrowth. Cell. Mol. Neurobiol. *30*, 1283–1292.

Woll, M.P., De Cotiis, D.A., Bewley, M.C., Tacelosky, D.M., Levenson, R., and Flanagan, J.M. (2011). Interaction between the D2 dopamine receptor and neuronal calcium sensor-1 analyzed by fluorescence anisotropy. Biochemistry *50*, 8780–8791.

Yamniuk, A.P., Silver, D.M., Anderson, K.L., Martin, S.R., and Vogel, H.J. (2007). Domain stability and metal-induced folding of calcium- and integrin-binding protein 1. Biochemistry *46*, 7088–7098.

